NJC

PAPER

View Article Online
View Journal | View Issue

Cite this: *New J. Chem.*, 2019, **43**, 6220

New dmso–ruthenium catalysts bearing N-heterocyclic carbene ligands for the ring-opening metathesis of norbornene

Thais R. Cruz,[a] Rodolpho A. N. Silva,[a] Antonio E. H. Machado, †[b] Benedito S. Lima-Neto,[c] Beatriz E. Goi[a] and Valdemiro P. Carvalho Jr *[a]

Received 14th February 2019,
Accepted 22nd March 2019

DOI: 10.1039/c9nj00810a

rsc.li/njc

Novel dimethyl sulfoxide ruthenium(II) complexes of N-heterocyclic carbenes [$RuCl_2$(S-dmso)$_2$(SIMes)] (**1**), [$RuCl_2$(S-dmso)$_2$(IMes)], (**2**) [$RuCl_2$(S-dmso)$_2$(SIDip)] (**3**), and [$RuCl_2$(S-dmso)$_2$(IDip)] (**4**) were successfully synthesized. The complexes **1–4** were characterized by elemental analysis, FTIR, UV-Vis, ^{1}H and ^{13}C NMR, and computational studies. The polynorbornene (polyNBE) syntheses *via* ROMP using the complexes **1–4** as pre-catalysts in the presence of ethyl diazoacetate (EDA) were evaluated under different [EDA]/[Ru] and [NBE]/[Ru] ratios, temperatures (25 and 50 °C) and times (5–60 min). Quantitative yields of polyNBEs using [NBE]/[EDA]/[Ru] = 5000/28/1 for 10 min at 25 °C were obtained. The order of magnitude of 10^5 g mol^{-1} for M_n and PDI values ranging from 1.2 to 3.5 were measured by SEC. An investigation combining experimental data and computational calculations was performed to elucidate the mechanism of ROMP of NBE mediated by the complexes **1–4** as pre-catalysts. The proposed mechanism suggests the occurrence of a dissociative reaction of the complexes **1–4**, losing a dmso ligand as the first step, resulting in a 14-electron species, which reacts with EDA to form the metal-carbene, followed by discoordination of the second dmso molecule for coordination of NBE.

1. Introduction

Catalytic olefin metathesis has become a powerful tool for the formation of carbon–carbon bonds in organic and polymer chemistry.[1,2] As a versatile method, olefin metathesis is involved in a wide range of organic transformations, such as ring-opening metathesis polymerization (ROMP),[3,4] ring-closing metathesis (RCM)[5,6] and acyclic-diene metathesis (ADMET) polymerization,[7,8] as well as tandem metathesis processes.[9,10] The scope of olefin metathesis has been extended by the development of well-defined catalytic systems and the success of this reaction has spurred intense investigation for new catalysts for this transformation.[11,12] A substantial number of ruthenium olefin metathesis catalysts have been developed and most of the efforts in designing new catalysts concentrated on finding more efficient catalytic systems, although most of them have focused only on modifying Grubbs catalysts.[13] For example, the catalysts were substituted by various types of ligands such as amines[14,15] and carbenes.[16–21]

On the other hand, ROMP has been studied with novel non-carbene Ru-based complexes, where the catalytic species is produced *in situ* by reaction with a carbene source. Our group has focused on the synthesis and reaction chemistry of *in situ* generated catalysts,[22–31] because their syntheses and reaction chemistry are of fundamental importance for a basic understanding in organometallic chemistry and might also lead to promising applications in catalysis. Besides that, there is a stimulating challenge in the search for simpler, cheaper, and perhaps Werner-type systems. In particular, we recently demonstrated that dimethyl sulfoxide–Ru complexes bearing different N-heterocyclic carbenes derived from cycloalkylamines have also contributed to the development of new catalysts for ROMP of norbornene (NBE).[32]

Here, we have explored an extension of the development of complexes of the type [$RuCl_2$(dmso)$_2$(NHC)] combining sulfoxides and N-heterocyclic carbenes (NHCs) as ancillary ligands to promote ROMP of NBE. The preparation and evaluation of dimethyl sulfoxide–ruthenium(II) complexes bearing N-heterocyclic carbenes with aryl substituents (Fig. 1) as catalyst precursors for ROMP of norbornene (NBE) have been reported. Herein we also report a systematic computational investigation of the thermodynamic feasibility of the dmso–ruthenium catalyzed ROMP mechanism.

[a] *Faculdade de Ciências e Tecnologia, UNESP Univ Estadual Paulista, CEP 19060-900, Presidente Prudente, SP, Brazil. E-mail: valdemiro.carvalho@unesp.br*
[b] *Instituto de Química, Universidade Federal de Uberlândia, P.O. Box 593, Uberlândia 38400-089, Minas Gerais, Brazil*
[c] *Instituto de Química de São Carlos, Universidade de São Paulo, CP 780, 13560-970, São Carlos, SP, Brazil*
† During his stay as Visiting Professor at the Programa de Pós-Graduação em Ciência e Tecnologia, at Universidade Federal de Goiás, Catalão, Goiás, Brazil.

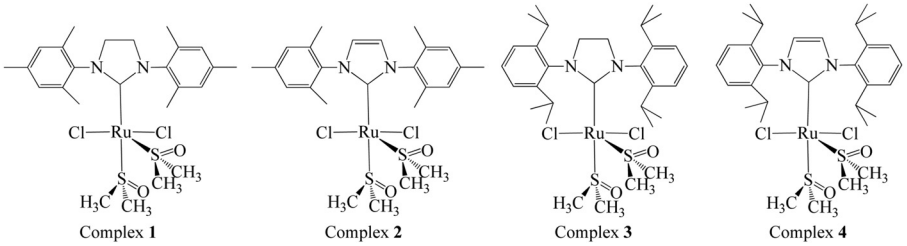

Fig. 1 Illustration of the dimethyl sulfoxide–ruthenium(II)–NHC carbene complexes **1–4**.

2. Experimental

2.1. General remarks

Unless otherwise stated, all syntheses, polymerizations and manipulations were performed under nitrogen atmosphere following standard Schlenk techniques. Solvents were distilled from appropriate drying agents and deoxygenated prior to use. Ruthenium(III) chloride hydrate ($RuCl_3{\cdot}xH_2O$), norbornene (NBE), and ethyl diazoacetate (EDA) were obtained from Aldrich and used as acquired. Imidazol(in)ium salts IMes·HCl, IDip·HCl, SIMes·HCl, and SIDip·HCl were synthesized according to published procedures.[33] Other commercially available reagents were used without further purification. The $[RuCl_2(S\text{-dmso})_3(O\text{-dmso})]$ complex was prepared following the literature and its purity was checked by satisfactory elemental analysis and spectroscopic examination (NMR, FTIR, and EPR).[34]

2.2. Analyses

Elemental analyses were performed with a PerkinElmer CHN 2400 at the Elemental Analysis Laboratory of Institute of Chemistry – USP. Electronic paramagnetic resonance (EPR) X-band/~9.85 GHz (Bruker EMX plus) measurements were carried out in a rectangular cavity with 100 kHz magnetic field modulation and 4 G of modulation amplitude at 77 K. The FTIR spectra were obtained in CsI pellets (1 : 100) on a Bomem FTIR MB 102. Electronic spectra were recorded on a Shimadzu (model UV-1800) spectrophotometer, using 1 cm path length quartz cells. The ^1H and ^{13}C NMR spectra were obtained in $CDCl_3$ at 298 K on a Bruker DRX-400 spectrometer of 9.4 T operating at 400.13 and 100.62 MHz, respectively. Chemical shifts are listed in parts per million downfield from TMS and are referenced from the solvent peaks or TMS. The complexes (10 mg) were dissolved in $CDCl_3$ that was previously degassed *via* a Tygon® tube (~600 mL) into the NMR tube. The molecular weights and the molecular weight distribution of the polymers were determined by gel permeation chromatography using a Shimadzu Prominence LC system equipped with a LC-20AD pump, a DGU-20A5 degasser, a CBM-20A communication module, a CTO-20A oven at 40 °C and a RID-10A detector equipped with two Shimadzu columns (GPC-805: 30 cm, Ø = 8.0 mm). The retention time was calibrated with standard monodispersed polystyrene using HPLC-grade THF as an eluent at 40 °C with a flow rate of 1.0 mL min^{-1}.

2.3. General procedure for the preparation of NHC–Ru complexes

An oven-dried 100 mL round-bottom flask equipped with a magnetic stirring bar and capped with a three-way stopcock was charged with a 1,3-diarylimidazol(in)ium salt (IMes, SIMes, IDip or SIDip) (1 equiv.), 95% sodium hydride (1.2 equiv.) and a catalytic amount of potassium *tert*-butoxide. The reactor was purged of air by applying three vacuum/argon cycles before dry THF was added. The resulting suspension was stirred for 2 h at room temperature, it was then allowed to settle for 1 h. The supernatant solution was filtered through Celite and transferred using a cannula under inert atmosphere into a two neck 100 mL round-bottom flask equipped with a magnetic stirring bar and capped with a three-way stopcock containing a solution of $[RuCl_2(S\text{-dmso})_3(O\text{-dmso})]$ (1 equiv.) in dry CH_2Cl_2 (10 mL). After 4 h of stirring at room temperature, the solvent was evaporated under vacuum. The residue was washed with *n*-pentane (20 mL) and dried under high vacuum.

2.3.1. $[RuCl_2(S\text{-dmso})_2(SIMes)]$ (complex 1). $[RuCl_2(S\text{-dmso})_3(O\text{-dmso})]$ complex (350 mg, 0.72 mmol), SIMes (307 mg, 1 mmol), and THF (50 mL) afforded 368 mg (81%) of the title complex as a yellow solid: anal. calculated for $C_{25}H_{38}Cl_2N_2O_2RuS_2$ was 47.31 C, 6.03 H and 4.41% N; found: 47.45 C, 6.23 H and 4.22% N. (a) UV-Vis: $\lambda_{max(n)}$ (nm), $\varepsilon_{max(n)}$ [M^{-1} cm^{-1}]: $\lambda_{max(1)}$ (253), $\varepsilon_{max(1)}$ [4837]; $\lambda_{max(2)}$ (370), $\varepsilon_{max(2)}$ [389]; (b) FTIR (CsI): ν_x (cm^{-1}): νC=C (1552), νC=N (1649), νS=O (1102, 1022), νRu–S (428), νRu–Cl (314); (c). ^1H NMR (400 MHz, $CDCl_3$): δ = 2.23 (s, 6 H, *para*-CH_3 Mes), 2.34 (s, 12 H, *ortho*-CH_3 Mes), 3.31 (s, 12 H, CH_3 S-dmso), 5.35 (s, 4 H, CH_2 imidazolic ring[4,5]), 7.39 (s, 4 H, *meta*-CH) ppm. ^{13}C NMR (100 MHz, $CDCl_3$): 16.8 (*ortho*-CH_3), 21.6 (*para*-CH_3), 42.2 (CH_2N), 46.0 (CH_3-S-dmso), 124.6 (*meta*-CH), 131.9 (*ipso*-C), 134.6 (*ortho*-C), 139.5 (*para*-C), 146.4 (Im-C2) ppm. EPR: no signal was observed.

2.3.2. $[RuCl_2(S\text{-dmso})_2(IMes)]$ (complex 2). $[RuCl_2(S\text{-dmso})_3(O\text{-dmso})]$ complex (350 mg, 0.72 mmol), IMes (205 mg, 1 mmol), and THF (50 mL) afforded 374 mg (82%) of the title complex as a yellow solid: anal. calculated for $C_{25}H_{36}Cl_2N_2O_2RuS_2$ was 47.46 C, 5.74 H and 4.43% N; found: 47.42 C, 5.54 H and 4.58% N. (a) UV-Vis: $\lambda_{max(n)}$ (nm), $\varepsilon_{max(n)}$ [M^{-1} cm^{-1}]: $\lambda_{max(1)}$ (245), $\varepsilon_{max(1)}$ [8437]; $\lambda_{max(2)}$ (375), $\varepsilon_{max(2)}$ [651]; (b) FTIR (CsI): ν_x (cm^{-1}): νC=C (1552), νC=N (1644), νS=O (1102, 1018), νRu–S (428), νRu–Cl (312); (c). ^1H NMR (400 MHz, $CDCl_3$): δ = 1.78 (s, 6 H, *para*-CH_3 Mes), 2.10 (s, 12 H, *ortho*-CH_3 Mes), 3.44 (s, 12 H, CH_3, S-dmso), 6.93 (s, 2 H, CH imidazolic ring[4,5]), 7.10 (s, 4 H, *meta* CH) ppm. ^{13}C NMR (100 MHz, $CDCl_3$): 17.1 (*ortho*-CH_3), 21.1 (*para*-CH_3), 46.1 (CH_3-S-dmso), 125.8 (Im-C4,5), 128.3 (*meta*-C), 130.1 (C_{ar}), 133.8 (C_{ar}), 134.4 (C_{ar}), 142.1 (Im-C2) ppm. EPR: no signal was observed.

2.3.3. $[RuCl_2(S\text{-dmso})_2(SIDip)]$ (complex 3). $[RuCl_2(S\text{-dmso})_3(O\text{-dmso})]$ complex (350 mg, 0.72 mmol), SIDip (391 mg, 1 mmol),

and THF (50 mL) afforded 375 mg (73%) of the title complex as a yellow solid: anal. calculated for $C_{31}H_{50}Cl_2N_2O_2RuS_2$ was 51.80 C, 7.01 H and 3.90% N; found: 52.02 C, 6.98 H and 3.73% N (a) UV-Vis: $\lambda_{max(n)}$ (nm), $\varepsilon_{max(n)}$ [M^{-1} cm^{-1}]: $\lambda_{max(1)}$ (254), $\varepsilon_{max(1)}$ [4239]; $\lambda_{max(2)}$ (370), $\varepsilon_{max(2)}$ [291]; (b) FTIR (CsI): ν_x (cm^{-1}): νC═C (1549), νC═N (1651), νS═O (1102, 1017), νRu–S (428), νRu–Cl (314); (c). ^{1}H NMR (400 MHz, $CDCl_3$): δ 1.21 [d, 12 H, CH(CH_3)$_2$], 1.38 [d, 12 H, CH(CH_3)$_2$], 3.10 [sept, 4 H, CH(CH_3)$_2$], 3.46 [s, 12 H, S-dmso], 4.86 [s, 4 H, CH_2 imidazolic ring[4,5]], 7.21–7.41 [m, 6 H, aryl-CH] ppm. ^{13}C NMR (100 MHz, $CDCl_3$): 24.1 (CH(CH_3)$_2$), 25.6 (CH(CH_3)$_2$), 29.1 (CH(CH_3)$_2$), 41.1 (CH_2N), 46.2 (CH_3, S-dmso), 125.1 (*meta*-CH), 129.6 (*para*-CH), 131.6 (*ipso*-CH), 146.5 (Im-C2) ppm. EPR: no signal was observed.

2.3.4. [$RuCl_2$(S-dmso)$_2$(IDip)] (complex 4). [$RuCl_2$(S-dmso)$_3$-(O-dmso)] complex (350 mg, 0.72 mmol), IDip (389 mg, 1 mmol), and THF (50 mL) afforded 352 mg (68%) of the title complex as a yellow solid: anal. calculated for $C_{31}H_{48}Cl_2N_2O_2RuS_2$ was 51.94 C, 6.75 H and 3.91% N; found: 52.02 C, 6.61 H and 3.84% N. (a) UV-Vis: $\lambda_{max(n)}$ (nm), $\varepsilon_{max(n)}$ [M^{-1} cm^{-1}]: $\lambda_{max(1)}$ (254), $\varepsilon_{max(1)}$ [7100]; $\lambda_{max(2)}$ (376), $\varepsilon_{max(2)}$ [1013]; (b) FTIR (CsI): ν_x (cm^{-1}): νC═C (1548), νC═N (1638), νS═O (1102, 1025), νRu–S (428), νRu–Cl (313); (c). ^{1}H NMR (400 MHz, $CDCl_3$): δ 1.21 [d, 12 H, CH(CH_3)$_2$], 1.29 [d, 12 H, CH(CH_3)$_2$], 2.51 [sept, 4 H, CH(CH_3)$_2$], 3.43 [s, 12 H, dmso], 7.35 [s, 2 H, CH imidazolic ring[4,5]], 7.41 (d, $^3J_{HH}$ = 6.4 Hz, 4H, *meta*-CH), 7.52 (t, $^3J_{HH}$ = 6.4 Hz, 2H, *para*-CH) ppm. ^{13}C NMR (100 MHz, $CDCl_3$): 24.0 (CH(CH_3)$_2$), 24.5 (CH(CH_3)$_2$), 29.0 (CH(CH_3)$_2$), 46.0 (CH_3, S-dmso), 124.6 (Im-C4,5), 125.2 (*meta*-CH), 127.9 (*ipso*-C), 130.0 (*para*-C), 132.0 (*ortho*-C), 145.2 (Im-C2) ppm EPR: no signal was observed.

2.4. Computation details

The structures of the compounds under study were optimized and had their vibrational frequencies calculated using density functional theory (DFT) at the level of the functional M06,[35] implemented in Gaussian 09,[36] using the basis set DGDZVP.[37] The presence of the solvent in the optimizations was simulated using the IEFPCM model.[38] From the analysis of the thermodynamic parameters obtained by the analysis of the vibrational spectra of the complexes and their different possible intermediates, it was possible to evaluate the ROMP mechanism initiated by the complexes **1–4**.

2.5. ROMP procedure

In a typical ROMP experiment, 1.1 μmol of the complex was dissolved in $CHCl_3$ (2 mL) with an appropriate amount of monomer (NBE), followed by addition of a carbene source (EDA). The polymerization was performed for different periods of time (5–60 min). The reaction mixture was stirred at 25 or 50 °C in a silicon oil bath. At room temperature, 10 mL of methanol was added and the precipitated polymer was filtered, washed with methanol and dried in a vacuum oven at 40 °C up to constant weight. The reported yields are average values from catalytic runs performed at least three times and the listed values are the arithmetic averages. The isolated polyNBEs were dissolved in THF for GPC data.

3. Results and discussion

3.1 Synthesis and characterization of the complexes

The preparation of complexes **1–4** was rather straightforward and could be achieved *via* reaction between [$RuCl_2$(S-dmso)$_3$-(O-dmso)] and the respective carbene (Scheme 1). Prior to the complexation step, the NHC precursors (IMes, SIMes, IDip or SIDip) were suspended in dry THF and deprotonated with sodium hydride in the presence of a catalytic amount of potassium *tert*-butoxide at room temperature. Within 2 h, the initially white solution became progressively pale yellow. Once the deprotonation step was completed, the suspensions were allowed to settle down and the inorganic byproduct was filtered off, along with any unreacted starting materials. The deprotonated imidazolium salts were reacted with an equimolar amount of [$RuCl_2$(S-dmso)$_3$(O-dmso)] complex to obtain the complexes **1–4** (Scheme 1). The products were isolated as microcrystalline yellow powders in good yields (68–82%) by simple filtration and washing, but were not suitable for single X-ray diffraction analysis. Even though the solid [$RuCl_2$(dmso)$_2$(NHC)] complexes have not been elucidated by X-ray diffraction of monocrystals, their structures have been well described by elementary analysis and spectroscopic techniques, such as FTIR, UV-Vis, and RMN.

The five-coordinated nature of the new complexes with the general formula of [$RuCl_2$(dmso)$_2$(NHC)] in the solid state was supported by the satisfactory analytical results that are in good agreement with the assigned formulation. The absence of a signal in the electron paramagnetic resonance (EPR) spectrum of the complexes **1–4** suggested the presence of a low spin d^6 electronic configuration with +2 oxidation state of ruthenium.

The infrared spectra were similar, with two strong bands in the region of 1102–1018 cm^{-1} assigned to the ν(S═O) stretching vibrations. S-Bonded dmso was evident from Ru–S stretching around 428 cm^{-1}. These bands now support linkage of dmso to the ruthenium metal centre through sulphur, following the literature.[39,40] Bands in 1548–1552 cm^{-1} were attributed to ν(C═C) of the imidazole ring. The band in the region of 314 cm^{-1} was attributed to ν(Ru–Cl) asymmetric stretching vibrations, respectively, suggesting two *trans*-positioned Cl^- ligands.

The ^{1}H NMR spectra in $CDCl_3$ for the complexes **1–4** are given in the Experimental section. The peaks in the range 1.0–2.4 ppm are assignable to the CH_3 group hydrogens from the mesityl or diisopropylphenyl substituents. The singlet around 3.3–3.5 ppm

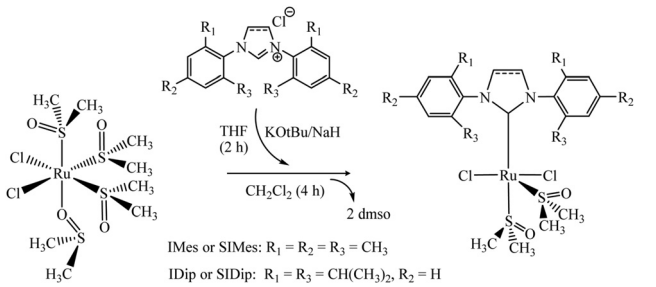

Scheme 1 Synthesis protocol of dimethyl sulfoxide ruthenium complexes bearing NHC ligands.

is assigned to the methyl groups of the S-bonded dmso. The chemical shifts observed around 4.6–7.3 ppm for complexes as singlets are assigned to the hydrogens present in the $C_{4,5}$ carbons of the imidazole ring. Finally, the signal of hydrogen of the C_2 carbon of the imidazole ring did not appear in the complexes **1–4** as expected, confirming the NHC coordination to the ruthenium centre. In the ^{13}C NMR spectra, carbon peaks between 24.0 and 147.0 ppm for complexes **1–4** were observed.

The five-coordinated complexes can exhibit two common structural isomers, labeled as trigonal bipyramid (TBp) and square pyramid (SP). Analyzing the structural optimization results of the complexes **1–4** from computational studies, it was observed that the TBp configuration represents the minimum energy structure for each of these complexes (Fig. 2). Relevant bond distances and angles of the studied complexes are presented in Table 1. With respect to the S-dmso ligands, one of them is considerably distant from the Ru centre in all complexes, which may probably reveal an easy substitution in the ROMP mechanism. The theoretical calculations corroborate with the FTIR and NMR data obtained in this study, which suggested that the two chloride ligands are *trans*-positioned.

Electronic spectra of the complexes **1–4** have been recorded in the 200–700 nm range in CH_2Cl_2 (Fig. 3). The electronic spectra of the complexes **1–4** show a band around 253 nm corresponding to intra-ligand $\pi \rightarrow \pi$ transition and another band of lower energy in the region 370 nm assignable to $Ru^{II} \rightarrow$ S-dmso charge transfer transitions. The absorption spectra of the complexes **1–4** are quite similar, showing the same amounts of bands at practically the same absorption maxima. This similarity is a strong indication that the four complexes have the same geometric structure with a similar qualitative configuration of the molecular orbitals.

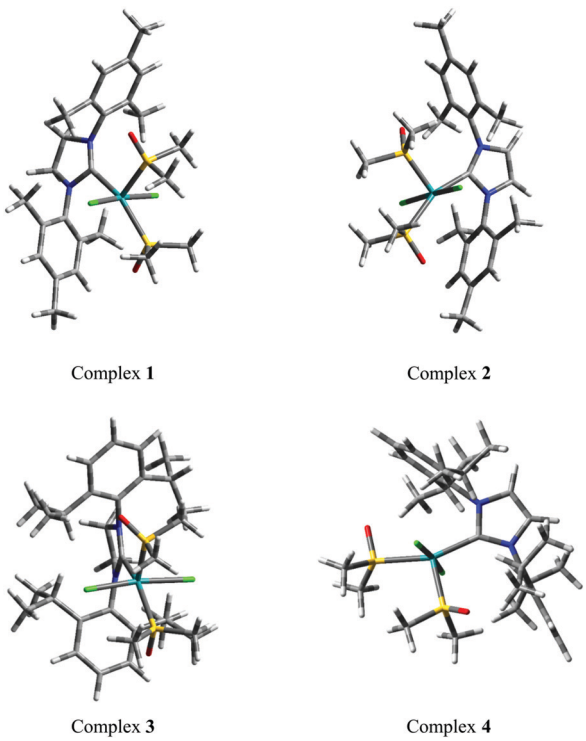

Fig. 2 Views of the optimized structures of complexes **1–4**.

Table 1 Theoretical data of relevant geometrical parameters of the studied complexes. For reference, for the atom numbering see Fig. 2

Geometrical parameter	Complex **1**	Complex **2**	Complex **3**	Complex **4**
Ru–Cl(62)	2.4635	2.4694	2.4593	2.4501
Ru–Cl(63)	2.4600	2.4576	2.4604	2.4629
Ru–S(51)	2.2722	2.3390	2.2714	2.2772
Ru–S(52)	2.4823	2.4099	2.4829	2.4465
Ru–C(3)	2.0855	2.0442	2.0942	2.1179
Cl(62)–Ru–Cl(63)	173.167	172.907	172.015	177.963

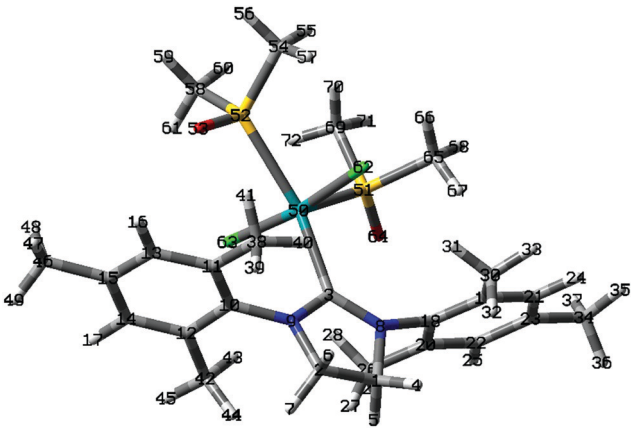

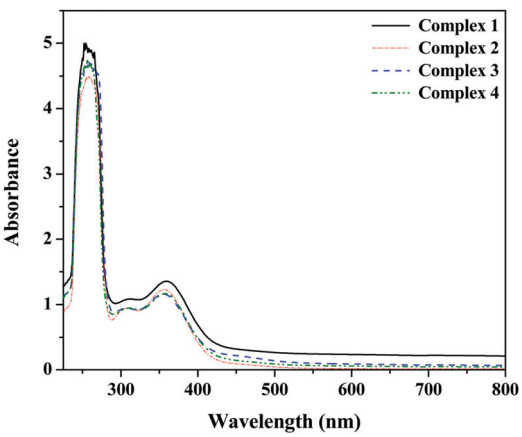

Fig. 3 Electronic spectra of the complexes **1–4** in degassed CH_2Cl_2 solution at room temperature ([Ru] = 0.1 mmol L^{-1}).

3.2. ROMP reactions

In order to assess the catalytic efficiency of dimethyl sulfoxide ruthenium(II) complexes **1–4**, ROMP of norbornene (NBE) was attempted in $CHCl_3$ in different [NBE]/[EDA]/[Ru] ratios at 25 or 50 °C (Scheme 2).

Fig. 4 shows the variation in the yield values of the isolated polymers as a function of time (5–60 min) for reactions with [NBE]/[Ru] = 5000 and [EDA]/[Ru] = 28 at 25 °C. Plotting the isolated polymer yields as a function of time (Fig. 4), first an increase is observed in the range of 5–10 min, followed by a drop of yield for 15–60 min, perhaps due to secondary reactions, such intermolecular chain-transfer or backbiting, when the

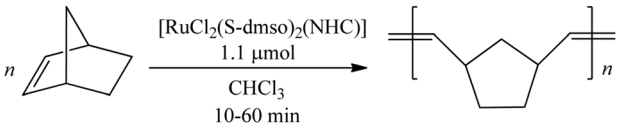

Scheme 2 ROMP of NBE catalysed by Ru–dmso complexes **1–4**.

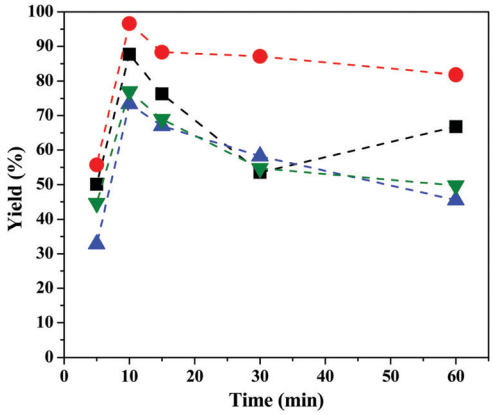

Fig. 4 Yield as a function of time for ROMP of NBE with complexes **1** (■), **2** (●), **3** (▲) and **4** (▼); [NBE]/[Ru] = 5000 and [EDA]/[Ru] = 28 (5 μL of EDA) in $CHCl_3$ at 25 °C.

reaction time is increased. This hypothesis is supported by the decreasing of the molecular weight and the increase of the PDI values of the polymers after 10 min of polymerization (Fig. 5).

The temperature at which the ROMP is conducted has strong influence over the outcome of the reaction and interferes in the kinetic and thermodynamic parameters of the polymerization. Generally, a low temperature favors the thermodynamics of polymerization, but disfavors the kinetics of the induction period. In this context, it is necessary to find a specific temperature that can tune these two parameters to obtain an induction period and propagation that are both more efficient. Thus, besides the catalytic tests performed at 25 °C, the polymerizations were also conducted at 50 °C using a [NBE]/[EDA]/[Ru] ratio of 5000/28/1 for 10 min (Fig. 6). The increase of temperature

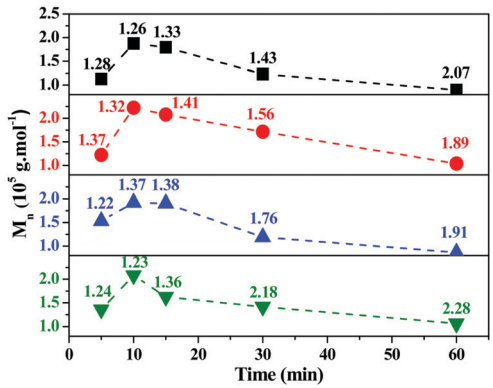

Fig. 5 M_n and PDI as a function of time for ROMP of NBE with complexes **1** (■), **2** (●), **3** (▲) and **4** (▼); [NBE]/[Ru] = 5000 and [EDA]/[Ru] = 28 in $CHCl_3$ at 25 °C.

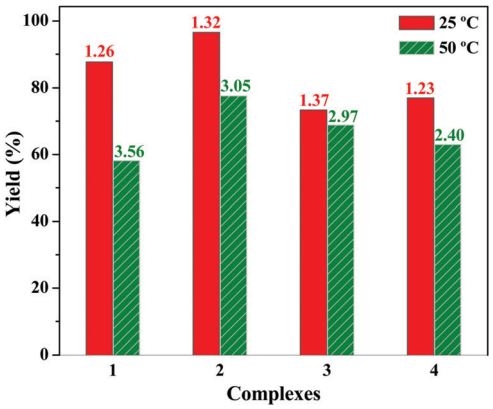

Fig. 6 Yield as a function of temperature, at 25 and 50 °C, for ROMP of NBE with complexes **1**, **2**, **3** and **4** in $CHCl_3$ for 10 min; [NBE]/[EDA]/[Ru] = 5000/28/1. The numbers correspond to the PDI values for each run.

produced lower yields of polyNBE with higher PDIs in relation to 25 °C in all cases. Considering that the catalytic activity of complexes **1–4** decreased at 50 °C, it is possible to infer that the release of ligands has no kinetic dependence during the induction period. The most favorable condition for a successful ROMP reaction using the complexes **1–4** is to conduct the polymerization under mild conditions with respect to temperature.[4]

It was found that the use of EDA was necessary to obtain any ROMP activity. Complexes **1–4** were completely inefficient in the absence of a diazo compound; however, when EDA was added to generate a metathetically active ruthenium-carbene species, the ROMP occurred with good yields. The catalytic activity of the complexes **1–4** increased with increase of the diazo compound/complex molar ratio up to [EDA]/[Ru] = 28 (volume of 5 μL), followed by a decrease in the yields to [EDA]/[Ru] > 28 (Fig. 7). Considering that complexes **1–4** have a similar profile when reacted with EDA, it is possible to affirm that the four complexes have the same pathway in the formation of the Ru carbene in the induction period. It should be noted that a very excessive amount of EDA ([EDA]/[Ru] > 28) provokes a decrease in the yields and molecular weight values with an increase in the PDI values, because of excessive coordination of EDA to the metal center (Fig. 8).[22,26] Thus, it is worth mentioning that the optimum EDA amount used as a carbene source was 5 μL ([EDA]/[Ru] = 28) for **1**, **2**, **3** and **4**.

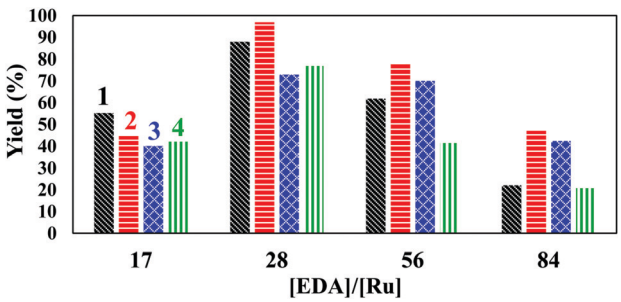

Fig. 7 Yield as a function of the [EDA]/[Ru] molar ratio for ROMP of NBE with complexes **1** (black), **2** (red), **3** (blue) and **4** (green); [NBE]/[Ru] = 5000 in $CHCl_3$ at 25 °C for 10 min.

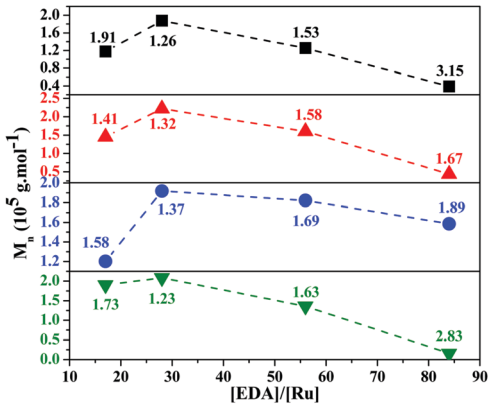

Fig. 8 M_n and PDI as a function of the [EDA]/[Ru] molar ratio for ROMP of NBE with complexes **1** (■), **2** (●), **3** (▲) and **4** (▼); [NBE]/[Ru] = 5000 in $CHCl_3$ at 25 °C for 10 min.

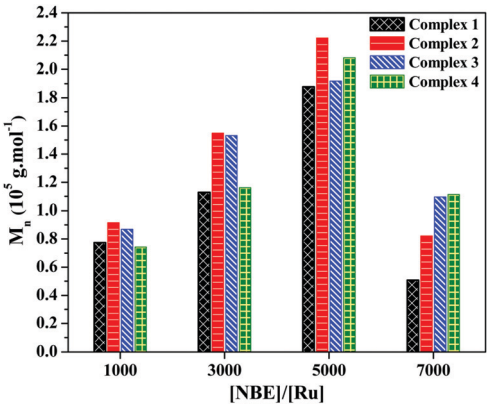

Fig. 10 M_n as a function of [NBE]/[Ru] ratio for ROMP of NBE with complexes **1** (black), **2** (red), **3** (blue) and **4** (green); [EDA]/[Ru] = 28 in $CHCl_3$ at 25 °C for 10 min.

ROMP is a process governed by thermodynamic equilibrium, in which the monomer/catalyst ratio can influence the thermodynamics of polymerization providing higher polymer production.[1–4] The monomer/complex ratio was varied in order to determine the optimum experimental conditions to achieve a smaller k_p/k_i ratio providing narrower molecular weight distribution polymers. The yields increase with increasing [NBE]/[Ru] molar ratio starting from 1000 with yields lower 20%, reaching semi-quantitative yields at 5000 for all complexes (Fig. 9). The increase in the monomer concentration contributed entropically to the ROMP process and improved the yields of polyNBE. For [NBE]/[Ru] = 7000, a decrease in the yields and molecular weight was observed (Fig. 10), which could be associated with the cage effect, which hinders the approach of the monomer to the metal centre.

In the ROMP experiments in the presence of 20-fold excess of dmso, the yields of polyNBE were less than 2% of polyNBE with [NBE]/[EDA]/[Ru] = 5000/28/1 for 10 min at 25 °C. Probably the presence of dmso in solution suppresses the leaving of the S-dmso ligand, preventing the ROMP reaction. These experiments suggest that the ROMP reaction using the complexes **1–4** depends on the lability of the S-dmso ligands, considering that the polymerization was inhibited in the presence of dmso.

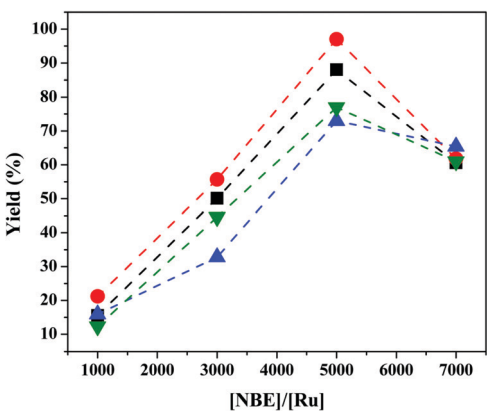

Fig. 9 Yield as a function of [NBE]/[Ru] ratio for ROMP of NBE with complexes **1** (■), **2** (●), **3** (▲) and **4** (▼); [EDA]/[Ru] = 28 in $CHCl_3$ at 25 °C for 10 min.

Since the complexes **1–4** are five-coordinated species, theoretically the ROMP may occur *via* two distinct mechanisms: associative or dissociative (Fig. 11). An analysis of the thermodynamic parameters calculated from quantum-mechanical data corroborates the dissociation of the S-dmso ligands, as suggested by experiments in the presence of dmso. The obtained values suggest that the mechanism should involve the elimination of both S-dmso ligands coordinated to the complex, especially in the reactions involving complexes **1** and **3**, once the coordination of the EDA in the five-coordinated species *via* an associative path is not a probable event to happen (reaction **I**) (Table 2). On the other hand, although the elimination of the first S-dmso has $\Delta G > 0$, this is a possible process, since, by its magnitude, the energy required to activate it can be provided by the thermal agitation of the medium itself (reaction **II**). Similar tendency occurs when the coordination of the NBE to the carbene complex with no S-dmso ligand in the coordination sphere is considered (reaction **V**). In addition, considering that the path that involves the formation of the metathetically active $\{RuCl_2(NHC)(=CHCO_2Et)\}$ *via* a dissociative mechanism involves several concerted reactions, it is very likely that the overall thermodynamic parameters for the process are favourable.

Considering the global equation $[RuCl_2(dmso)_2(NHC)]$ + EDA + NBE → $\{RuCl_2(NHC)(=CHCO_2Et)(NBE)\}$ + 2 dmso and based on the thermodynamic parameters calculated for the individual reactions *via* the dissociative mechanism, the thermomechanical parameters for the overall reaction can be estimated (Table 3). These data suggest that the formation reactions of the complexes $\{RuCl_2(NHC)(=CHCO_2Et)(NBE)\}$ *via* the dissociative mechanism are thermodynamically favorable in all cases.

The catalytic efficiency of the complexes **1–4** bearing aryl-substituted NHC ligands are much better than those of dimethyl sulfoxide–ruthenium(II) complexes bearing cycloalkyl-substituted NHC carbenes.[32] We believe that this difference in the reactivity of these complexes is directly related to the structural differences present in both cases. The cycloalkyl-substituted NHC–Ru–dmso complexes have a square base pyramidal geometry with the two S-dmso ligands (π-acceptor) *trans*-positioned to the chloride (π-donor) on the equatorial axis. This configuration provides

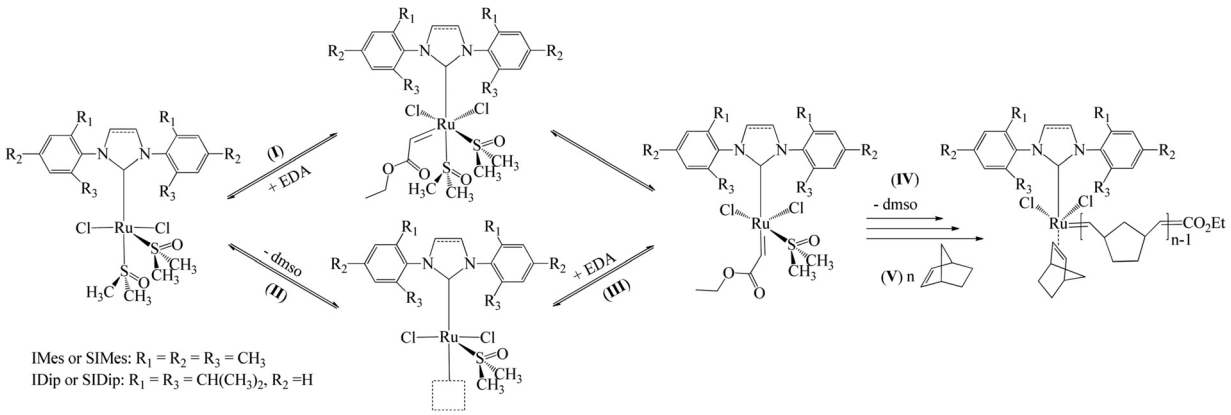

Fig. 11 Proposed mechanism for ROMP by the $[RuCl_2(dmso)_2(NHC)]$ complexes.

Table 2 Calculated thermodynamic parameters at 298 K for each possible reaction in the ROMP mechanism mediated by complexes **1–4**

	Units: kJ mol^{-1}			
Reaction	Complex **1**	Complex **2**	Complex **3**	Complex **4**
I	ΔG = +2901.41 ΔH = +2827.60 $T\Delta S$ = −73.81	ΔG = −200.48 ΔH = −260.33 $T\Delta S$ = −59.85	ΔG = +2885.07 ΔH = +2827.14 $T\Delta S$ = −57.93	ΔG = −155.14 ΔH = −227.94 $T\Delta S$ = −72.80
II	ΔG = +3.11 ΔH = +61.09 $T\Delta S$ = +57.98	ΔG = +15.90 ΔH = +81.04 $T\Delta S$ = +65.14	ΔG = +1.24 ΔH = +62.71 $T\Delta S$ = +61.48	ΔG = +24.64 ΔH = +85.71 $T\Delta S$ = +61.07
III	ΔG = −218.29 ΔH = −279.00 $T\Delta S$ = +60.71	ΔG = −234.53 ΔH = −309.67 $T\Delta S$ = −75.14	ΔG = −229.01 ΔH = −282.20 $T\Delta S$ = −53.19	ΔG = −211.93 ΔH = −277.38 $T\Delta S$ = −65.45
IV	ΔG = +17.53 ΔH = +75.07 $T\Delta S$ = +57.53	ΔG = +32.68 ΔH = +95.78 $T\Delta S$ = +63.10	ΔG = +12.99 ΔH = +76.13 $T\Delta S$ = +63.14	ΔG = −1.87 ΔH = +55.19 $T\Delta S$ = +57.06
V	ΔG = +4.25 ΔH = −48.52 $T\Delta S$ = −52.77	ΔG = +8.42 ΔH = −41.33 $T\Delta S$ = −49.75	ΔG = +11.91 ΔH = −44.12 $T\Delta S$ = −56.03	ΔG = +14.16 ΔH = −35.67 $T\Delta S$ = −49.83

Table 3 Calculated overall thermodynamic parameters for the formation reaction of EDA and NBE containing complexes at 298 K

Complex	ΔG (kJ mol^{-1})	ΔH (kJ mol^{-1})	$T\Delta S$ (kJ mol^{-1})
1	−193.40	−191.35	+2.05
2	−177.52	−174.18	+3.34
3	−202.88	−187.48	+15.40
4	−175.00	−172.16	+2.84

great stability to these complexes due to the *trans*-cooperative Cl → Ru → S-dmso effects, which hinders the release of the dmso ligands from the coordination sphere by retarding the ROMP reaction. This observation is supported by the increase in catalytic activity with increasing temperature in this case, showing the kinetic dependence involved in the discoordination of the dmso ligands. On the contrary, the complexes **1–4** are found to be more dynamic in solution, since these *trans*-cooperative effects in the equatorial axis are not present in these complexes. The trigonal bipyramidal geometry obtained for the complexes **1–4**, a configuration exerted by the steric hindrance of the NHC with aryl substituents, provided a greater lability of the dmso ligands. Note that the NHC provokes a *trans* influence on the axial dmso ligand, evidenced by the longer bond length. These effects imposed by geometry favored the reactivity of complexes **1–4** in ROMP reactions.

4. Conclusions

The complexes **1–4** were successfully synthesized and characterized by infrared, UV-vis and ^{1}H and ^{13}C NMR spectroscopy, elementary analysis, and computational studies. It was concluded that two dmso molecules have been replaced by a N-heterocyclic carbene in the coordination sphere, leading to five-coordinated complexes with TBp-geometry. The complexes **1–4** demonstrated good catalytic activities as catalytic precursors in ROMP of NBE at 25 °C with a [NBE]/[Ru] ratio of 5000 in the presence of 5 μL of EDA. The electronic synergism induced by the strong σ-donation of the NHC and the π-acceptor olefin (NHC → Ru → NBE) contributed to the good reactivity of the complexes **1–4**.

An experimental/theoretical study proposes that the ROMP reaction initiated by $[RuCl_2(dmso)_2(NHC)]$ follows a dissociative mechanism. The first step is a dissociative reaction of the initial complex releasing the first dmso ligand, followed by the coordination of EDA to form the metal carbene species. This species loses the second dmso molecule in an endothermic reaction driven by entropy changes, leaving the Ru center able to receive the NBE molecule. From this study, it was significant to observe a non-dmso complex as the catalytic species, where the electronic effect of the NHC carbene is operative throughout the ROMP reaction.

Conflicts of interest

There are no conflicts to declare.

Acknowledgements

The authors are indebted to FAPESP (Proc. 2013/10002-0) for the financial support.

References

1 *Handbook of Metathesis*, ed. R. H. Grubbs, Wiley-VCH, Weinheim, 1st edn, 2003.
2 *Olefin Metathesis: Theory and Practice*, ed. K. Grela, Wiley, Hoboken, 1st edn, 2014.
3 C. Slugovc, *Macromol. Rapid Commun.*, 2004, **25**, 1283–1297.
4 W. Bielawski and R. H. Grubbs, *Prog. Polym. Sci.*, 2007, **32**, 1–29.
5 R. H. Grubbs and S. Chang, *Tetrahedron*, 1998, **54**, 4413–4450.
6 J. M. Berlin, S. D. Goldberg and R. H. Grubbs, *Angew. Chem., Int. Ed.*, 2006, **45**, 7591–7595.
7 S. Demel, C. Slugovc, F. Stelzer, K. Fodor-Csorba and G. Galli, *Macromol. Rapid Commun.*, 2003, **24**, 636–641.
8 H. Mutlu, L. Montero de Espinosa and M. A. R. Meier, *Chem. Soc. Rev.*, 2011, **40**, 1404–1445.
9 M. Schuster and S. Blechert, *Angew. Chem., Int. Ed.*, 1997, **36**, 2036–2056.
10 Y. Borguet, X. Sauvage, G. Zaragoza, A. Demonceau and L. Delaude, *Beilstein J. Org. Chem.*, 2010, **6**, 1167–1173.
11 R. R. Schrock, *Angew. Chem., Int. Ed.*, 2006, **45**, 3748–3759.
12 R. H. Grubbs, *Angew. Chem., Int. Ed.*, 2006, **45**, 3760–3765.
13 G. C. Vougioukalakis and R. H. Grubbs, *Chem. Rev.*, 2010, **110**, 1746–1787.
14 T. M. Trunka, E. L. Dias, M. W. Day and R. H. Grubbs, *ARKIVOC*, 2002, **13**, 28–41.
15 M. S. Sanford, J. A. Love and R. H. Grubbs, *J. Am. Chem. Soc.*, 2001, **123**, 6543–6554.
16 J. Huang, E. D. Stevens, S. P. Nolan and J. L. Petersen, *J. Am. Chem. Soc.*, 1999, **121**, 2674–2678.
17 V. Sashuk, L. H. Peeck and H. Plenio, *Chem. – Eur. J.*, 2010, **16**, 3983–3993.
18 S. Wolf and H. Plenio, *J. Organomet. Chem.*, 2010, **695**, 2418–2422.
19 X. Bantreil, R. A. M. Randall, A. M. Z. Slawin and S. P. Nolan, *Organometallics*, 2010, **29**, 3007–3011.
20 J. P. Moerdyk and C. W. Bielawski, *Organometallics*, 2011, **30**, 2278–2284.
21 E. L. Rosen, D. H. Sung, Z. Chen, V. M. Lynch and C. W. Bielawski, *Organometallics*, 2010, **29**, 250–256.
22 J. M. E. Matos and B. S. L. Neto, *J. Mol. Catal. A: Chem.*, 2004, **222**, 81–85.
23 J. M. E. Matos and B. S. L. Neto, *J. Mol. Catal. A: Chem.*, 2006, **259**, 286–291.
24 J. L. S. Sá and B. S. L. Neto, *J. Mol. Catal. A: Chem.*, 2009, **304**, 187–190.
25 J. L. S. Sá, L. H. Vieira, E. S. P. Nascimento and B. S. L. Neto, *Appl. Catal., A*, 2010, **374**, 194–200.
26 V. P. Carvalho, C. P. Ferraz and B. S. Lima-Neto, *J. Mol. Catal. A: Chem.*, 2010, **333**, 46–53.
27 H. K. Chaves, C. P. Ferraz, V. P. Carvalho Jr and B. S. L. Neto, *J. Mol. Catal. A: Chem.*, 2014, **385**, 46–53.
28 L. R. Fonseca, E. S. P. Nascimento, J. L. S. Sá and B. S. L. Neto, *New J. Chem.*, 2015, **39**, 4063–4069.
29 R. A. N. Silva, P. Borim, L. R. Fonseca, B. S. Lima Neto, J. L. S. Sá and V. P. Carvalho Jr, *Catal. Lett.*, 2017, **147**, 1144–1152.
30 M. B. A. Afonso, T. R. Cruz, Y. F. Silva, J. C. A. Pereira, A. E. H. Machado, B. E. Goi, B. S. Lima-Neto and V. P. Carvalho Jr, *J. Organomet. Chem.*, 2017, **851**, 225–234.
31 P. Borim, B. S. Lima Neto, B. E. Goi and V. P. Carvalho Jr, *Inorg. Chim. Acta*, 2017, **456**, 171–178.
32 A. H. S. Idehara, P. D. S. Gois, H. Fernandez, B. E. Goi, A. E. H. Machado, B. S. Lima-Neto and V. P. Carvalho Jr, *Mol. Catal.*, 2018, **448**, 135–143.
33 A. J. Arduengo III, R. Krafczyk, R. Schmutzler, H. A. Craig, J. R. Goerlich, W. J. Marshall and M. Unverzagt, *Tetrahedron*, 1999, **55**, 14523–14534.
34 I. P. Evans, A. Spencer and G. Wilkinson, *J. Chem. Soc., Dalton Trans.*, 1973, **2**, 204–209.
35 Y. Zhao and D. G. Truhlar, *Theor. Chem. Acc.*, 2006, **120**, 215–241.
36 M. J. Frisch, G. W. Trucks, H. B. Schlegel, G. E. Scuseria, M. A. Robb, J. R. Cheeseman, G. Scalmani, V. Barone, B. Mennucci, G. A. Petersson, H. Nakatsuji, M. Caricato, X. Li, H. P. Hratchian, A. F. Izmaylov, J. Bloino, G. Zheng, J. L. Sonnenberg, M. Hada, M. Ehara, K. Toyota, R. Fukuda, J. Hasegawa, M. Ishida, T. Nakajima, Y. Honda, O. Kitao, H. Nakai, T. Vreven, J. A. Montgomery, Jr., J. E. Peralta, F. Ogliaro, M. Bearpark, J. J. Heyd, E. Brothers, K. N. Kudin, V. N. Staroverov, T. Keith, R. Kobayashi, J. Normand, K. Raghavachari, A. Rendell, J. C. Burant, S. S. Iyengar, J. Tomasi, M. Cossi, N. Rega, J. M. Millam, M. Klene, J. E. Knox, J. B. Cross, V. Bakken, C. Adamo, J. Jaramillo, R. Gomperts, R. E. Stratmann, O. Yazyev, A. J. Austin, R. Cammi, C. Pomelli, J. W. Ochterski, R. L. Martin, K. Morokuma, V. G. Zakrzewski, G. A. Voth, P. Salvador, J. J. Dannenberg, S. Dapprich, A. D. Daniels, O. Farkas, J. B. Foresman, J. V. Ortiz, J. Cioslowski and D. J. Fox, *Gaussian 09, Revision E.01*, Gaussian, Inc., Wallingford CT, 2013.
37 N. Godbout, D. R. Salahub, J. Andzelm and E. Wimmer, *Can. J. Chem.*, 1992, **70**, 560–571.
38 J. Tomasi, B. Mennucci and E. Cancès, *J. Mol. Struct.*, 1999, **464**, 211–226.
39 E. Alessio, *Chem. Rev.*, 2004, **104**, 4203–4242.
40 M. Calligaris and O. Carugo, *Chem. Rev.*, 1996, **153**, 83–154.